Available online at www.sciencedirect.com
SCIENCE DIRECT®
Journal of Sound and Vibration 291 (2006) 1080–1103
JOURNAL OF SOUND AND VIBRATION
www.elsevier.com/locate/jsvi

Enhancement of the accuracy of the (P–ω) method through the implementation of a nonlinear robust observer

G.A. Kfoury[a], N.G. Chalhoub[a,*], N.A. Henein[a], W. Bryzik[b]

[a]*Department of Mechanical Engineering, Wayne State University, Detroit, MI 48202, USA*
[b]*US Army Tank-Automotive RDE Center, AMSTA-R, Warren, MI 48397-5000, USA*

Received 22 October 2004; received in revised form 5 July 2005; accepted 10 July 2005
Available online 9 September 2005

Abstract

The (P–ω) method is a model-based approach developed for determining the instantaneous friction torque in internal combustion engines. This scheme requires measurements of the cylinder gas pressure, the engine load torque, the crankshaft angular displacement and its time derivatives. The effects of the higher order dynamics of the crank-slider mechanism on the measured angular motion of the crankshaft have caused the (P–ω) method to yield erroneous results, especially, at high engine speeds. To alleviate this problem, a nonlinear sliding mode observer has been developed herein to accurately estimate the rigid and flexible motions of the piston-assembly/connecting-rod/crankshaft mechanism of a single cylinder engine. The observer has been designed to yield a robust performance in the presence of disturbances and modeling imprecision.

The digital simulation results, generated under transient conditions representing a decrease in the engine speed, have illustrated the rapid convergence of the estimated state variables to the actual ones in the presence of both structured and unstructured uncertainties. Moreover, this study has proven that the use of the estimated rather than the measured angular displacement of the crankshaft and its time derivatives can significantly improve the accuracy of the (P–ω) method in determining the instantaneous engine friction torque.
© 2005 Elsevier Ltd. All rights reserved.

*Corresponding author. Tel.: +1 313 577 3753; fax: +1 313 577 8789.
E-mail address: nchalhoub@eng.wayne.edu (N.G. Chalhoub).

0022-460X/$ - see front matter © 2005 Elsevier Ltd. All rights reserved.
doi:10.1016/j.jsv.2005.07.029

Nomenclature

A_i, m_i cross-sectional area and mass of the ith beam element, respectively

D, d_1 cylinder bore diameter and journal bearing diameter, respectively

EI_i, GJ_i flexural rigidity and torsional stiffness of the ith beam element, respectively

F_{rm}, F_{rv} represent the friction forces stemming from the boundary-mixed and the hydrodynamic lubrication regimes of the piston rings, respectively.

F_{sk} friction force due to the hydrodynamic lubrication regime of the piston skirt.

F_{vt} friction force of the valve train.

$\underset{\sim}{F}(q,\dot{q})$ vector containing inertial, stiffness and gravitational acceleration terms

g, ρ gravitational acceleration and density, respectively

$\bar{I}_j$ inertia tensor of the jth rigid body

$(\underset{\sim}{I},\underset{\sim}{J},\underset{\sim}{K})$ unit vectors along the axes of the inertial coordinate system

L_i, L_{skirt} length of the ith beam element and the piston skirt, respectively

$\underset{\sim}{M}(q)$ inertia tensor in the detailed model of the crank-slider mechanism

n_{crg}, n_{valve} number of compression rings and valves, respectively

P_{gas}, $P_{e,crg}$ cylinder gas pressure and elastic pressure of the compression ring, respectively

$\underset{\sim}{Q}^{NC}$ nonconservative generalized force vector

SL, w_{crg} valve spring load and average width of the compression ring, respectively

T_a friction torque of the auxiliaries and unloaded bearings

T_f engine friction torque generated by the detailed model of the crank-slider mechanism

T_{fa} engine friction torque generated by the $(P$–$\omega)$ method based on θ and its time derivatives as generated by the detailed model

T_{fe} engine friction torque generated by the $(P$–$\omega)$ method based on the estimated θ_{m_e} and $\dot{\theta}_{m_e}$ by the nonlinear observer

$T_i^{i'}$ represents the location of $O_{i'}$ and the orientation of $(x_{i'}, y_{i'}, z_{i'})$ with respect to (x_i, y_i, z_i)

T_{j-1}^{j} 4×4 matrix defining the origin and orientation of the jth coordinate system with respect to the $(j$–$1)$th frame in the nominal rigid body configuration of the crankshaft

T_{lb}, T_{load} friction torque of the loaded bearings and engine load torque, respectively

V_p, μ piston velocity and dynamic viscosity of the oil, respectively

W_{cr}, W_{cs} out-of-plane transverse deformations of the connecting-rod and the crankshaft, respectively

$(x_{\tilde{3}'}, y_{\tilde{3}'}, z_{\tilde{3}'})$ represents a floating coordinate system whose origin is fixed at $z_3 = L_3/2$

$(x_{6'_e}, y_{6'_e}, z_{6'_e})$ represents a floating coordinate system whose origin is fixed at $x_6 = L_6$

θ,β,γ angular displacements of the crankshaft, the connecting rod and the piston, respectively

ϕ, Φ_i torsional vibration and ith eigenfunction of the crankshaft, respectively

$\theta_m, q_{1_m}, q_{2_m}$ variables simulating the measured angular displacement along with the first and second elastic mode of the crankshaft

$\underset{\sim}{\bar{\omega}}_j$ rotation vector of the jth rigid body

$()_{cr}$, $()_{cs}$ "cr" and "cs" subscripts refer to variables associated with the connecting-rod and the crankshaft, respectively

$()_{cwi}$ a "cwi" subscript indicates a variable associated with the ith counterweight

$()_e$, $()_m$ "e" and "m" subscripts indicate estimated and measured values of the state variable, respectively

$()_{fl}$, $()_{gr}$ "fl" and "gr" subscripts denote variables associated with the flywheel and the crank gear, respectively

$()_p$, $()_{pr}$ "p" and "pr" subscripts refer to variables associated with the piston and the piston rings, respectively

$()_{sk}$ a "sk" subscript refers to a variable associated with the piston skirt

1. Introduction

Frictional losses of reciprocating and rotating engine components have a significant effect on the overall engine performance. Common approaches for determining the average value of these losses over the entire engine cycle are the Willan line method, the Morse method and the indicated work method. These techniques are limited in their scope of application to steady-state modes of operation of the engine [1].

Other approaches such as the "movable bore" method [2] and the "fixed sleeve" method [3] have been developed to provide direct measurement of the instantaneous frictional losses of the piston-ring assembly. Both techniques require extensive modifications of the engine structure and suffer from the problem of separating the friction force from all other forces that might be exerted on the system such as the gas force and the inertial forces.

The instantaneous mean effective pressure (IMEP) method [4] yields indirect measurement of the instantaneous piston-ring assembly frictional losses. This approach requires accurate measurements of the connecting-rod force, the cylinder gas pressure and the crankshaft angular velocity. It is based on a simplified rigid body model of the piston and a portion of the connecting-rod.

Similarly, the $(P-\omega)$ method [5] represents a model-based approach in which the instantaneous friction torque of the engine is computed by relying on a rigid body model of the piston-assembly/connecting-rod/crankshaft mechanism. This methodology requires accurate measurements of the cylinder gas pressure, the engine load torque, the crankshaft angular position and its time derivatives.

The salient feature of both the $(P–\omega)$ method and the IMEP technique stems from the fact that they do not require structural modifications of the engine. They are both applicable under transient and steady-state modes of operation of the engine. Furthermore, they can be implemented under either motoring or firing engine conditions. Note that these schemes have no provision in their formulations to account for the structural deformations of the crank-slider mechanism. However, the measurement of the rotary motion of the crankshaft, needed for the implementation of these methods, is usually obtained by using an optical encoder. The latter emits a signal reflecting the measurement noise, the contribution of the higher order dynamics of the system along with the rigid body behavior of the crankshaft. As a consequence, both schemes have lead to erroneous results by yielding positive numerical values for the friction force/torque during specific periods of the engine cycle. Moreover, the friction curve is shown to become hardly recognizable at high engine speeds due to the effects of inertial forces and the crank-slider structural deformations. Chalhoub and his co-workers [6] have demonstrated that the accuracy of the $(P–\omega)$ method can be significantly improved if the measured angular displacement and its time derivatives can be modified to solely represent the rigid body motion of the crankshaft.

A low-pass filter is commonly used on the crankshaft angular velocity in order to attenuate the noise level and the unwanted contribution of the higher order dynamics of the system. The use of a filtered angular velocity in the $(P–\omega)$ method has been examined in Ref. [7] and found to yield unacceptable estimation of the engine friction torque. This is because the nonlinearities of the crank-slider mechanism have introduced superharmonic and combination resonance frequencies in the angular displacement of the crankshaft. The use of a low-pass filter causes severe attenuation in the superharmonic resonance frequencies, which constitute an important part of

the rigid body behavior of the crankshaft that is needed by the (P–ω) method to accurately predict the engine friction torque. Moreover, the filtered signals would still be contaminated by the combination resonance frequency components appearing in the low-frequency range, which is commonly assumed to be dominated by the frequency components of the rigid body motion of the crank-slider mechanism. Therefore, the nonlinearities of the system have rendered the low-pass filter technique to be inapplicable. This is because the filtered angular velocity signal does not accurately represent the actual rigid body motion of the crankshaft.

To overcome this difficulty, Taraza and his co-workers [8] mounted two optical encoders to measure the angular displacements at both ends of the crankshaft. These measurements are then used along with a lumped mass model of the crank-slider mechanism to extract the rigid body angular velocity of the crankshaft. The latter is then implemented in the (P–ω) method to determine the engine friction torque. This procedure has significantly improved the accuracy of the (P–ω) method. However, its drawback stems from the fact that it can only be applied under steady-state mode of operation of the engine and cannot take into consideration more than one elastic mode of the crankshaft.

The focus of the current work is to enhance the accuracy of the (P–ω) method, in determining the instantaneous engine friction torque, by relying on estimated rather than measured angular displacement of the crankshaft and its time derivatives. It should be stressed that this approach is consistent with recent studies that preferred estimated state variables over measured ones in order to improve the performance of the controller [9] or to reduce the effect of observation spillover in the active control of flexible structures [10]. To achieve our goal, a nonlinear robust observer is developed herein to estimate the rigid and flexible motions of the crankshaft in the presence of both structured and unstructured uncertainties of the system [11–14]. Moreover, the structure of the proposed observer allows for the simultaneous estimation of several elastic modes of the crankshaft.

Several observer design methodologies, based on the variable structure systems (VSS) theory, have been proposed for a large class of dynamical systems with bounded nonlinearities and/or uncertainties [11–14]. These observers do not require exact knowledge of the plant and their design is solely based on knowing the upper bounds of the system uncertainties and/or nonlinearities.

Walcott and Zak [11] developed a variable structure observer for systems with observable linear parts and bounded nonlinearities and/or uncertainties. Slotine et al. [12] proposed sliding observers for general nonlinear systems. They discussed in detail the design procedure of VSS observers for nonlinear systems expressed in the companion form. Furthermore, they provided a general guidance on how to determine the gains of sliding mode observers for nonlinear systems expressed in the general form. The estimator, developed in the current study, consists of a VSS observer having a structure similar to the one proposed by Slotine et al. [12] for general nonlinear systems.

The physical system considered in this study consists of a piston-assembly/connecting-rod/crankshaft mechanism for a single cylinder engine. The dynamic model of the system is described in the following section. Subsequently, the proposed nonlinear robust observer is presented. In Section 4, the performance of the observer, in accurately estimating the rigid and flexible motions of the crank-slider mechanism in the presence of disturbances and model imprecision, is assessed. In Section 5, the procedure for determining the instantaneous engine friction torque based on the

(P–ω) method is presented. In addition, the digital simulation results, presented in Section 5, demonstrate the enhancement in the accuracy of the (P–ω) method that can be realized by computing the instantaneous friction torque based on estimated rather than measured rigid body motion of the crankshaft. Finally, the work is summarized and the main contributions are highlighted.

2. Dynamic model of the crank-slider mechanism

A detailed model is used herein to determine the combined rigid and flexible motions of the piston-assembly/connecting-rod/crankshaft mechanism for a single cylinder four-stroke internal combustion engine (see Fig. 1). The derivation ignores the piston slap and the piston tilting. It treats the piston as a rigid body and computes the instantaneous friction torque, T_f, based on the engine component friction formulations derived by Rezeka and Henein [15]. It should be emphasized that any other engine friction model could have equally served the purpose of this study. Furthermore, the results generated by the detailed model are used in this study as a basis for comparison and they are referred to throughout the manuscript as the "exact" results.

The model takes into consideration the first three elastic modes for each of the torsional vibration, ϕ, and the out-of-plane transverse deformation, W_{cs}, of the crankshaft. Note that ϕ and W_{cs} are highly coupled. For any two adjacent beam elements of the crankshaft (see Fig. 1), what may constitute the torsional vibration of one element becomes the slope of the transverse deformation of the other. The structural flexibility terms are discretized by using the assumed modes method [16]. The admissible functions in the ϕ and W_{cs} approximations are selected to be the eigenfunctions of the crankshaft, including the counterweights, the flywheel and the crank gear [17,18].

Since the connecting-rod is stiffer than the crankshaft then only the first elastic mode of its out-of-plane transverse deformation, W_{cr}, is included in the derivations. The admissible function used in the approximation of W_{cr} is considered to be the eigenfunction of a pinned–pinned beam, which is readily available in the literature [19].

The extended absolute position vectors of any point on the ith beam element of the crankshaft, the connecting-rod as well as the mass center of the piston can be expressed as

$$\left\{ \begin{matrix} r^{(i)\mathrm{T}} \\ \sim_{\mathrm{cs}} \end{matrix} |1 \right\}^{\mathrm{T}} = \left[\prod_{j=1}^{i} T_{j-1}^{j} \right] T_{i}^{i'} \{x_{i'} y_{i'} 0 |1\}^{\mathrm{T}}, \tag{1}$$

$$\left\{ \begin{matrix} r^{\mathrm{T}} \\ \sim_{\mathrm{cr}} \end{matrix} |1 \right\}^{\mathrm{T}} = T_0^3 T_3^{\tilde{3}'} T_{\tilde{3}'}^6 T_6^{6'} \{0 y_{6'} z_{6'} |1\}^{\mathrm{T}}, \tag{2}$$

$$\left\{ \begin{matrix} r^{\mathrm{T}} \\ \sim_{p} \end{matrix} |1 \right\}^{\mathrm{T}} = T_0^3 T_3^{\tilde{3}'} T_{\tilde{3}'}^6 T_6^{6'_e} T_{6'_e}^7 \{x_7^* y_7^* z_7^* |1\}^{\mathrm{T}}. \tag{3}$$

Next, the kinetic and potential energy expressions are determined from

$$\mathrm{K.E.} = \frac{1}{2} \sum_{i=1}^{5} \int_{m_i} \dot{r}_{\underset{\sim}{\mathrm{cs}}}^{(i)} . \dot{r}_{\underset{\sim}{\mathrm{cs}}}^{(i)} \, \mathrm{d}m_i + \frac{1}{2} \sum_{j} (m_j \dot{r}_{\underset{\sim}{j}} . \dot{r}_{\underset{\sim}{j}} + \bar{\omega}_{\underset{\sim}{j}}^{\mathrm{T}} \bar{I}_j \bar{\omega}_{\underset{\sim}{j}}) + \frac{1}{2} \int_{m_{\mathrm{cr}}} \dot{r}_{\underset{\sim}{\mathrm{cr}}} . \dot{r}_{\underset{\sim}{\mathrm{cr}}} \, \mathrm{d}m_{\mathrm{cr}}, \tag{4}$$

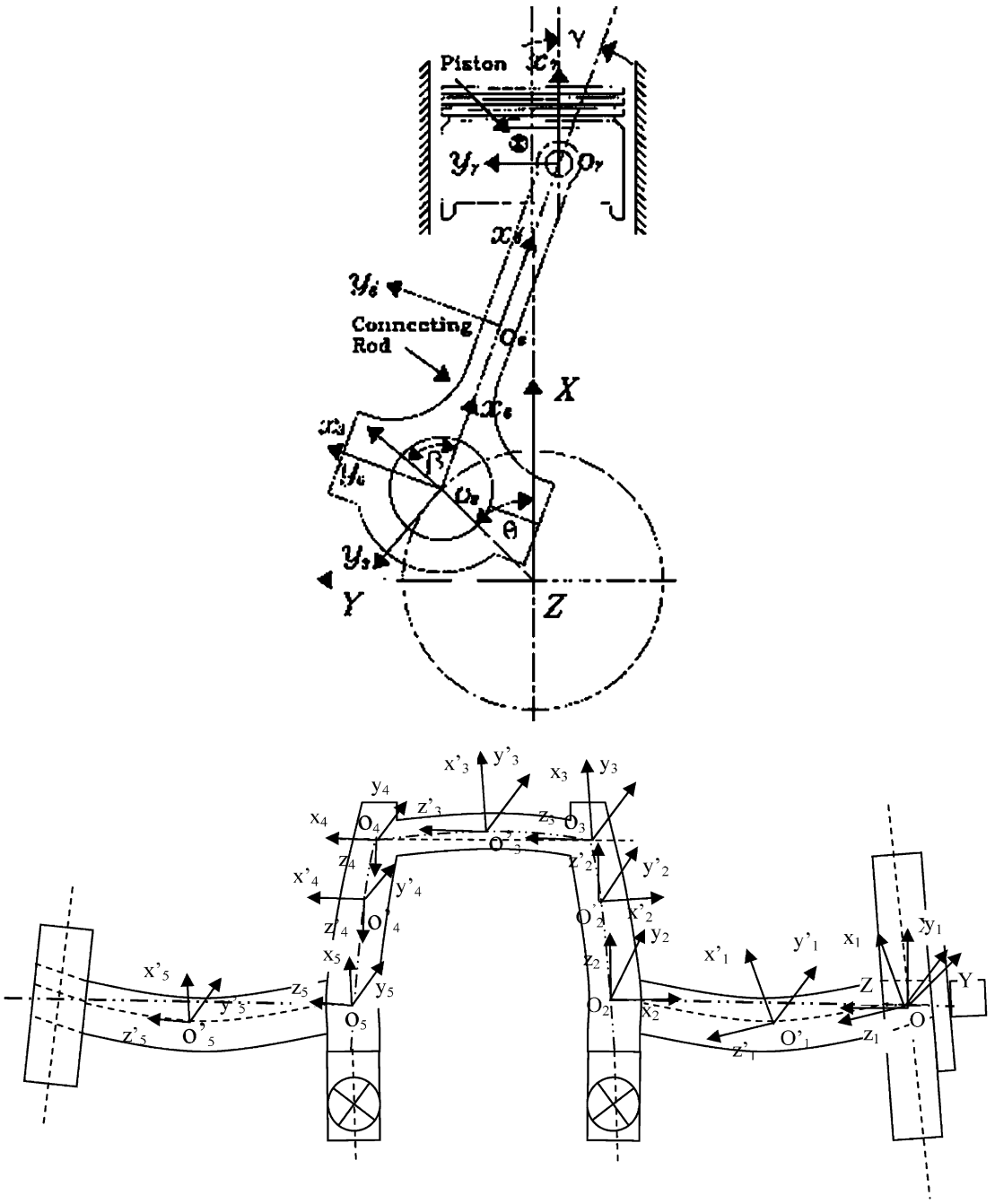

Fig. 1. Schematic of the piston-assembly/connecting-rod/crankshaft mechanism.

$$\text{P.E.} = \frac{1}{2}\sum_{i=1}^{5}\left[\int_0^{L_i} EI_i(W_{\text{cs},z_iz_i})^2\,\mathrm{d}z_i + \int_0^{L_i} GJ_i(\phi_{,z_i})^2\,\mathrm{d}z_i\right] + \frac{1}{2}\int_0^{L_6} EI_6(W_{\text{cr},x_6x_6})^2\,\mathrm{d}x_6$$
$$+ \sum_{i=1}^{5}\int_0^{L_i} \rho A_i g\,\underset{\sim}{I}\,.\underset{\sim}{r}_{\text{cs}}^{(i)}\,\mathrm{d}z_i + \int_0^{L_6} \rho A_6 g\,\underset{\sim}{I}\,.\underset{\sim}{r}_{\text{cr}}\,\mathrm{d}x_6 + \sum_j (m_j g\,\underset{\sim}{I}\,.\underset{\sim}{r}_j)$$
$$j = \text{fl}, \text{cwl}, \text{cw2}, \text{gr}, p, \tag{5}$$

where the datum line is considered to coincide with the inertial Z-axis (see Fig. 1). The virtual work done by the nonconservative generalized forces is

$$\delta W_{\text{NC}} = -P_{\text{gas}}A_p\,\underset{\sim}{I}\,.\delta\underset{\sim}{r}_p + \int_0^{L_2}\left\{\underset{\sim}{F}_{\text{ax}}^{(2)}.\left[-\frac{1}{2}\delta(W_{\text{cs},z_2}^2)\,\underset{\sim}{k}_2\right]\right\}\mathrm{d}z_2$$
$$+ \int_0^{L_4}\left\{\underset{\sim}{F}_{\text{ax}}^{(4)}.\left[-\frac{1}{2}\delta(W_{\text{cs},z_4}^2)\,\underset{\sim}{k}_4\right]\right\}\mathrm{d}z_4 + \int_0^{L_6}\left\{\underset{\sim}{F}_{\text{ax}}^{(6)}.\left[-\frac{1}{2}\delta(W_{\text{cr},x_6}^2)\underset{\sim}{i}_6\right]\right\}\mathrm{d}x_6 + \delta W_f$$
$$- T_{\text{load}}\,\underset{\sim}{K}.\left[-\delta W_{\text{cs},z_5}\,\underset{\sim}{i}_5 + W_{\text{cs},z_5}\delta\theta\,\underset{\sim}{j}_5 + (\delta\theta+\delta\phi)\,\underset{\sim}{k}_5\right]_{z_5=L_5}, \tag{6}$$

where the terms involving $\underset{\sim}{F}_{\text{ax}}^{(i)}$ reflect the stiffening effect induced by the centripetal acceleration of the system. δW_f is the virtual work done by the friction forces and torques. It is defined as follows

$$\delta W_f = -(F_{\text{rm}}+F_{\text{rv}})\delta\left[T_0^7(x_{\text{pr}}^*y_{\text{pr}}^*z_{\text{pr}}^*|1)^{\text{T}}\right] - F_{\text{vt}}\delta\left[T_0^7(x_7^*y_7^*z_7^*|1)^{\text{T}}\right]$$
$$- F_{\text{sk}}\delta\left[T_0^7(x_{\text{sk}}^*y_{\text{sk}}^*z_{\text{sk}}^*|1)^{\text{T}}\right] - (T_a+T_{\text{lb}})\left[\delta\theta + \frac{1}{2}\delta\phi\left(z_1=\frac{L_1}{2}\right) + \frac{1}{2}\delta\phi\left(z_5=\frac{L_5}{2}\right)\right]. \tag{7}$$

Note that the expressions for the friction forces and torques are adopted from the work done by Rezeka and Henein [15] (see Table 1).

Three coordinates θ, β and γ have been used herein to represent the rigid body motion of the crank-slider mechanism. To deal with the superfluous coordinates, the following two constraint equations are imposed to prevent the piston from tilting or from moving away from the centerline of the cylinder in the $\underset{\sim}{J}$-direction:

$$\underset{\sim}{\bar{\omega}}_p\,.\,\underset{\sim}{k}_7 = 0 \text{ and } \underset{\sim}{r}_p^*(t).\,\underset{\sim}{J} = \text{const.} \tag{8}$$

The equations of motion of the crank-slider mechanism are obtained by implementing the Lagrange principle. They consist of seven nonlinear, coupled, stiff, second-order ordinary differential equations, which can be written in the following compact form:

$$M(\underset{\sim}{q})\,\underset{\sim}{\ddot{q}} + \underset{\sim}{F}(\underset{\sim}{q},\underset{\sim}{\dot{q}}) = \underset{\sim}{Q}^{\text{NC}} + s_1^{\text{T}}(\underset{\sim}{q})\,\underset{\sim}{\lambda}, \tag{9}$$

where q is defined to be $(\theta, \beta, \gamma, q_1, q_2, q_3, q_4)^{\text{T}}$. s_1 is obtained by differentiating the constraint equations with respect to time and by writing the results as

$$s_1\,\underset{\sim}{\ddot{q}} + \underset{\sim}{s_2} = \underset{\sim}{0}. \tag{10}$$

Table 1
Frictional losses of the engine components

Ring	
Boundary-mixed	$F_{\mathrm{rm}} = 0.252\pi D n_{\mathrm{crg}} w_{\mathrm{crg}}(P + P_{e,\mathrm{crg}})(1 - \lvert\mathrm{Sin}(\theta)\rvert)$ $270^\circ \leqslant \theta \leqslant 450^\circ$
Viscous lubrication	$F_{\mathrm{rv}} = 23.0[\mu \lvert V_p \rvert w_{\mathrm{crg}}(P + P_{e,\mathrm{crg}})]^{1/2}(1.4 n_{\mathrm{crg}})D$
Skirt	$F_{\mathrm{sk}} = \mu V_p D L_{\mathrm{skirt}}/h$
Valve train	$F_{\mathrm{vt}} = 0.26 n_{\mathrm{valve}} \mathrm{SL}/\sqrt{\dot{\theta}}$
Auxiliaries and unloaded bearings	$T_a = 9.6\mu\dot{\theta}$
Loaded bearings	$T_{\mathrm{lb}} = 0.5(\pi/4)D^2 P \lvert\mathrm{Cos}(\theta)\rvert (d_1/2)/\sqrt{\dot{\theta}}$

The Lagrange multiplier vector, $\underset{\sim}{\lambda}$, is determined by implementing the scheme in Ref. [20]. It can be computed from

$$\underset{\sim}{\lambda} = -(s_1 M^{-1} s_1^{\mathrm{T}})^{-1}\left[\underset{\sim}{s_2} + s_1 M^{-1}\left(\underset{\sim}{Q}^{\mathrm{NC}} - \underset{\sim}{F}\right)\right]. \tag{11}$$

The equations of motion are converted in this study to a set of 14 first-order ordinary differential equations, which can be written as

$$\underset{14\times1}{\dot{\underset{\sim}{x}}} = \underset{14\times1}{\underset{\sim}{f}}(\underset{\sim}{x}(t), P_{\mathrm{gas}}, T_{\mathrm{load}}) = \begin{pmatrix} \underset{7\times1}{\dot{\underset{\sim}{q}}} \\ M^{-1}(\underset{\sim}{q}(t))\left\{-\underset{\sim}{F}(\underset{\sim}{q}, \dot{\underset{\sim}{q}}) + \underset{\sim}{Q}^{\mathrm{NC}} + s_1^{\mathrm{T}}(\underset{\sim}{q})\,\underset{\sim}{\lambda}\right\} \end{pmatrix}. \tag{12}$$

The state vector, $\underset{\sim}{x}(t)$, is defined to be $[\underset{\sim}{q}^{\mathrm{T}}\dot{\underset{\sim}{q}}^{\mathrm{T}}]^{\mathrm{T}}$. No closed form solution exists for these equations. Instead, they are solved numerically by using the Gear method with a variable-time step [21], which is well suited for stiff systems. The reader is referred to Ref. [17] for further details on the dynamic model of the crank-slider mechanism.

3. Design of a nonlinear observer

The robust nonlinear observer is designed herein to estimate $\theta(t), q_1(t), q_2(t)$ and their time derivatives in the presence of disturbances and model uncertainties. To achieve this goal, a nominal reduced order model of the crank-slider mechanism has been used in the design of the observer. This model ignores the third elastic mode of the crankshaft and treats the connecting-rod as a rigid body. The rationale is to examine the effects of unstructured uncertainties on the performance of the observer.

The Lagrange multipliers are approximated based on the rigid body equations of the crank-slider mechanism. Their expressions are determined from Eq. (11) after deleting all the entries and the terms associated with the structural flexibility of the system. Furthermore, the approximate expressions for the superfluous coordinates β, γ and their time derivatives with respect to θ, $\dot{\theta}$ and $\ddot{\theta}$ have been obtained from the rigid body constraint equations, which are determined from Eq. (8) after setting all the structural flexibility terms to zero. The derived approximate expressions are then used to eliminate $\underset{\sim}{\lambda}$ along with β, γ and their time derivatives from the θ, q_1 and q_2 equations, which are obtained from Eq. (9) after deleting all the terms involving q_3, q_4 and their time derivatives. The resulting θ, q_1 and q_2 equations are then converted to the following six first-order ordinary differential equations representing the state equations of the nominal model:

$$\dot{\underset{\sim}{\hat{x}}}_r(t) = \underset{\sim}{\hat{f}}(\underset{\sim}{\hat{x}}_r, P_{\text{gas}}, T_{\text{load}}), \tag{13}$$

where $\underset{\sim}{\hat{x}}_r$ is defined to be $[\theta, q_1, q_2, \dot{\theta}, \dot{q}_1, \dot{q}_2]^{\text{T}}$. Moreover, to further increase the structured uncertainties of the nominal model, all its parameters have been assigned numerical values that are 20% less than their exact values.

In designing the observer, the crankshaft motion is assumed to be measured at three different locations. This can be done by mounting an optical encoder at each end of the crankshaft and by

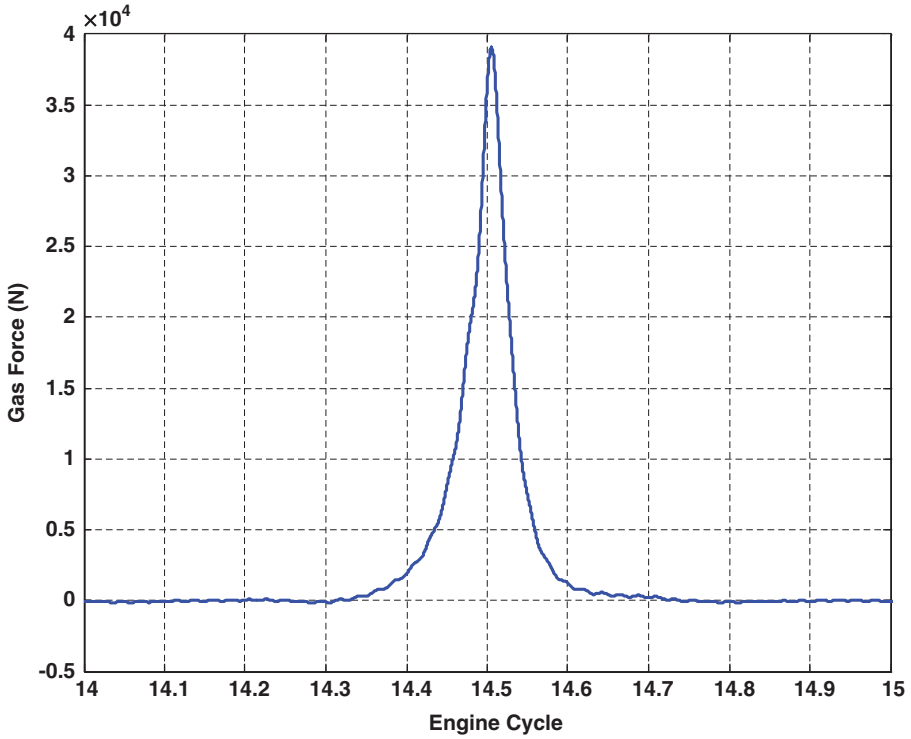

Fig. 2. Cylinder gas force.

using a noncontacting transducer to measure the torsional vibration at the first crankjournal. Therefore, the independent measurements, y_i's, can be expressed as

$$y_1(t) = \theta(t) + \sum_{i=1}^{n} \Phi_i(z_1 = 0) q_i(t), \tag{14a}$$

$$y_2(t) = \theta(t) + \sum_{i=1}^{n} \Phi_i(z_5 = L_5) q_i(t), \tag{14b}$$

$$y_3(t) = \sum_{i=1}^{n} \Phi_i(z_1^*) q_i(t). \tag{14c}$$

In the detailed model, n is assumed to be 3. However, the nominal model, used in the design of the estimator, only accounts for the first two elastic modes of the crankshaft. As a consequence, the measured signals can be related to the state variables of the nominal model through the

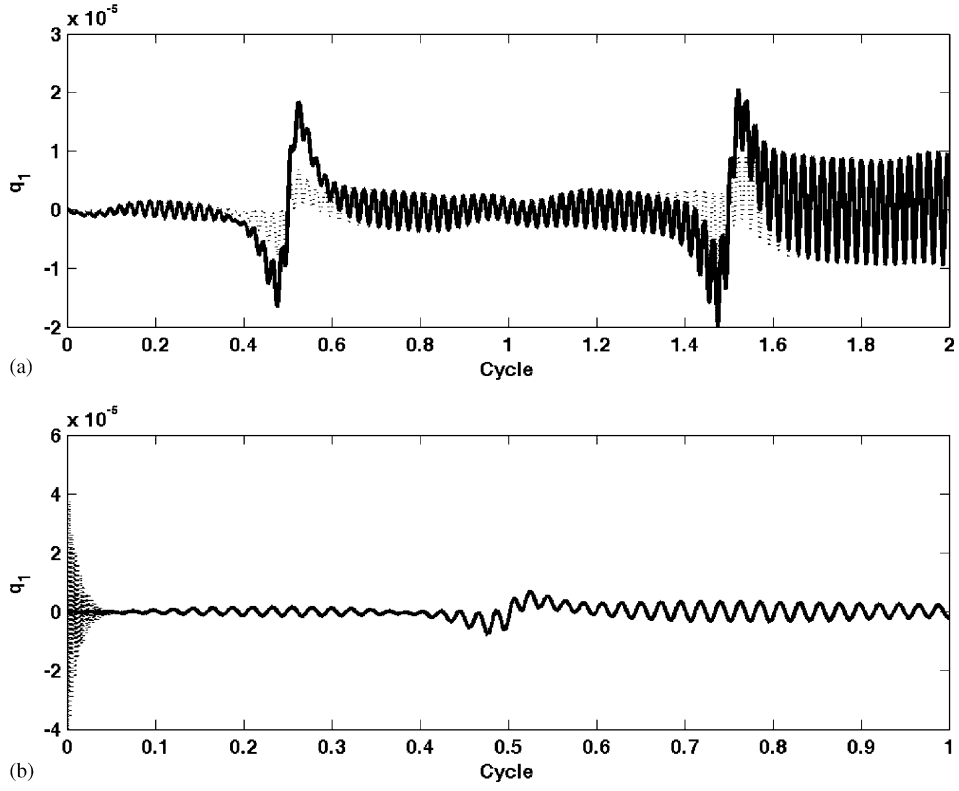

Fig. 3. First elastic mode of the crankshaft from case 1. (a) Exact (——) and measured (……), (b) measured (——) and estimated (……).

following approximate relationships:

$$\begin{pmatrix} y_1 \\ y_2 \\ y_3 \end{pmatrix} = \begin{bmatrix} 1 & \Phi_1(z_1 = 0) & \Phi_2(z_1 = 0) \\ 1 & \Phi_1(z_5 = L_5) & \Phi_2(z_5 = L_5) \\ 0 & \Phi_1(z_1^*) & \Phi_2(z_1^*) \end{bmatrix} \begin{pmatrix} x_{r1_m} = \theta_m \\ x_{r2_m} = q_{1_m} \\ x_{r3_m} = q_{2_m} \end{pmatrix} = \bar{C} \begin{pmatrix} x_{r1_m} \\ x_{r2_m} \\ x_{r3_m} \end{pmatrix}$$

$$\Rightarrow \begin{pmatrix} x_{r1_m} \\ x_{r2_m} \\ x_{r3_m} \end{pmatrix} = \bar{C}^{-1} \begin{pmatrix} y_1 \\ y_2 \\ y_3 \end{pmatrix}. \tag{15}$$

This approximation is justified when the contribution of the higher order dynamics is sufficiently small. It should be pointed out that the C matrix is nonsingular because the three measurements are independent signals. Moreover, the following expressions for $\dot{\theta}_m$, $\dot{q}_{1_m}$ and $\dot{q}_{2_m}$ have been used in this study for the sole purpose of establishing a basis for comparison for the

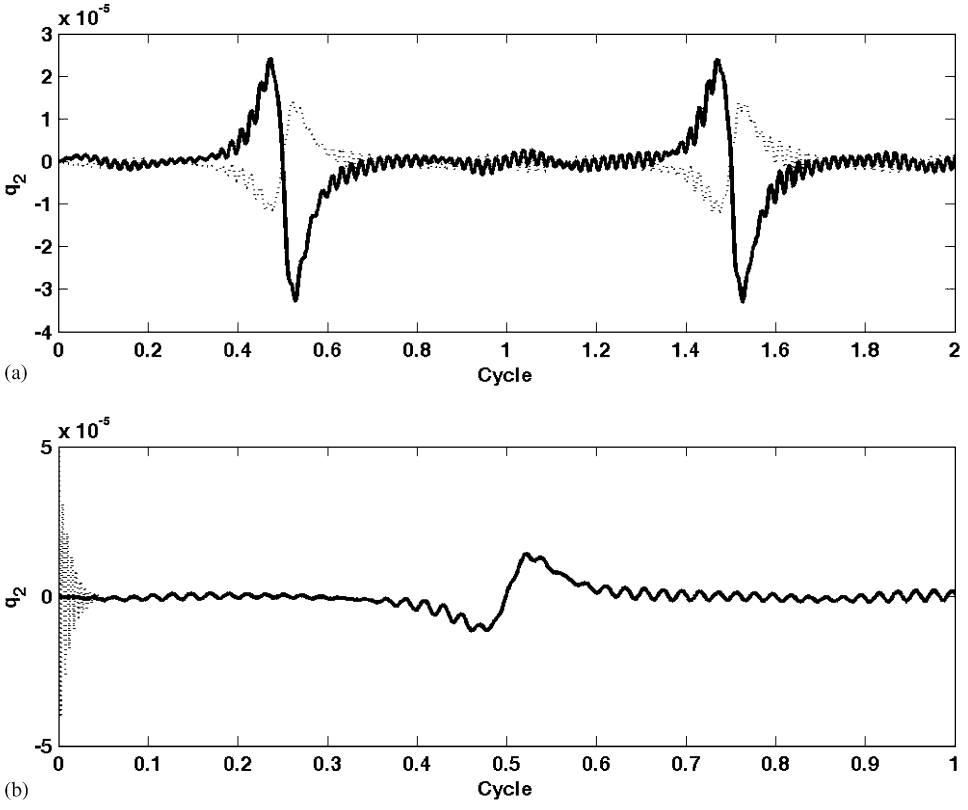

Fig. 4. Second elastic mode of the crankshaft from case 1. (a) Exact (——) and measured (……), (b) measured (——) and estimated (……).

estimated $\dot{\theta}_e$, $\dot{q}_{1_e}$ and $\dot{q}_{2_e}$:

$$\begin{pmatrix} x_{r4_m} \\ x_{r5_m} \\ x_{r6_m} \end{pmatrix} = \begin{pmatrix} \dot{\theta}_m \\ \dot{q}_{1_m} \\ \dot{q}_{2_m} \end{pmatrix} = \bar{C}^{-1} \begin{pmatrix} \dot{\theta} + \sum_{i=1}^{3} \Phi_i(z_1 = 0)\dot{q}_i(t) \\ \dot{\theta} + \sum_{i=1}^{3} \Phi_i(z_5 = L_5)\dot{q}_i(t) \\ \sum_{i=1}^{3} \Phi_i(z_1^*)\dot{q}_i(t) \end{pmatrix}. \tag{16}$$

In this work, the following three sliding surfaces are selected:

$$s_1 \triangleq \theta_e - \theta_m = \hat{x}_{r1} - x_{r1_m} = \tilde{x}_{r1}, \tag{17a}$$

$$s_2 \triangleq q_{1_e} - q_{1_m} = \hat{x}_{r2} - x_{r2_m} = \tilde{x}_{r2}, \tag{17b}$$

$$s_3 \triangleq q_{2_e} - q_{2_m} = \hat{x}_{r3} - x_{r3_m} = \tilde{x}_{r3}. \tag{17c}$$

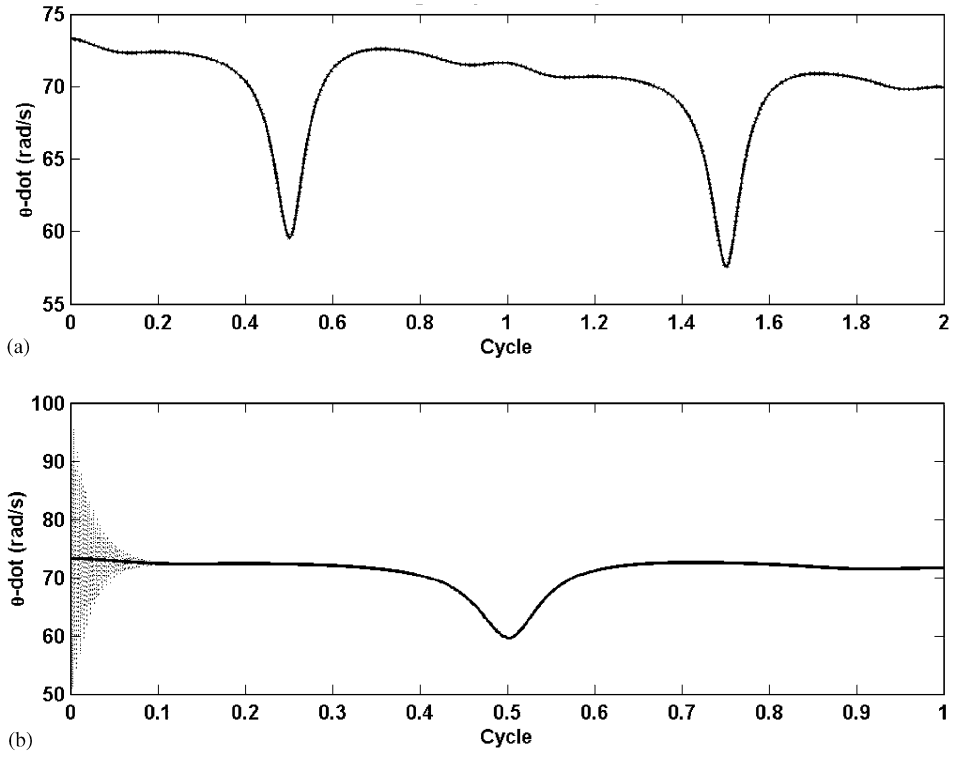

Fig. 5. Angular velocity of the crankshaft from case 1. (a) Exact (——) and measured (……), (b) measured (——) and estimated (……).

By adopting the observer structure developed by Slotine and co-workers in Ref. [12], the vector state equation of the estimator is obtained by modifying Eq. (13) as follows :

$$\dot{\hat{\underset{\sim}{x}}}_r(t) = \hat{\underset{\sim}{f}}\left(\hat{\underset{\sim}{x}}_r, P_{\text{gas}}, T_{\text{load}}\right) - \bar{k}_{6\times 3}\begin{pmatrix}\tilde{x}_{r1}\\ \tilde{x}_{r2}\\ \tilde{x}_{r3}\end{pmatrix} - k_{6\times 3}\begin{pmatrix}\text{sgn}(\tilde{x}_{r1})\\ \text{sgn}(\tilde{x}_{r2})\\ \text{sgn}(\tilde{x}_{r3})\end{pmatrix}. \tag{18}$$

Consequently, the estimation error vector equation becomes

$$\dot{\tilde{\underset{\sim}{x}}}_r(t) = \Delta\underset{\sim}{f}_r - \bar{k}_{6\times 3}\begin{pmatrix}\tilde{x}_{r1}\\ \tilde{x}_{r2}\\ \tilde{x}_{r3}\end{pmatrix} - k_{6\times 3}\begin{pmatrix}\text{sgn}(\tilde{x}_{r1})\\ \text{sgn}(\tilde{x}_{r2})\\ \text{sgn}(\tilde{x}_{r3})\end{pmatrix}, \tag{19}$$

where

$$\begin{aligned}\Delta\underset{\sim}{f}_r &= \begin{bmatrix}\tilde{x}_{r4} & \tilde{x}_{r5} & \tilde{x}_{r6} & \Delta f_{r4} & \Delta f_{r5} & \Delta f_{r6}\end{bmatrix}^{\text{T}}\\ &= \begin{bmatrix}\hat{x}_{r4}-x_8 & \hat{x}_{r5}-x_{11} & \hat{x}_{r6}-x_{12} & f_{r4}-f_8 & f_{r5}-f_{11} & f_{r6}-f_{12}\end{bmatrix}^{\text{T}}.\end{aligned} \tag{20}$$

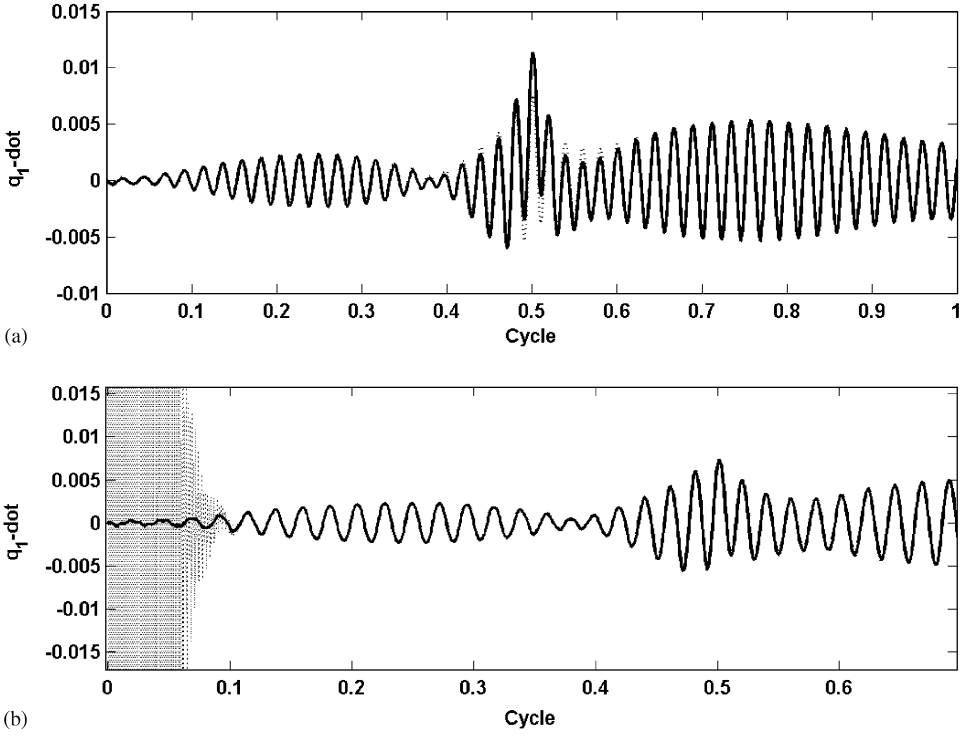

Fig. 6. $\dot{q}_1$ of the crankshaft from case 1. (a) Exact (——) and measured (……), (b) measured (——) and estimated (……).

The time derivative of the ith sliding surface can be expressed as

$$\dot{s}_i = \tilde{x}_{r(i+3)} - \sum_{j=1}^{3} \bar{k}_{ij}\tilde{x}_{rj} - \sum_{l=1}^{3} k_{il}\,\mathrm{sgn}(\tilde{x}_{rl}) \quad i = 1,\ 2,\ \text{and } 3. \tag{21}$$

It should be pointed out that the off-diagonal terms in k have been set to zero in the current study. The diagonal entries k_{11}, k_{22} and k_{33} are selected to satisfy the following sliding conditions:

$$\frac{1}{2}\frac{\mathrm{d}}{\mathrm{d}t}s_i^2\left(\underset{\sim}{\tilde{x}}_r, t\right) \leqslant -\eta_i|s_i| \quad i = 1,\ 2,\ \text{and } 3. \tag{22}$$

In addition, the k_{ii} terms must be positive so that the switching terms, $-k_{ii}\,\mathrm{sgn}(\tilde{x}_{ri})$'s, can force the system to remain on the sliding surfaces in the presence of both model imprecision and disturbances. This has led to the following expressions for the k_{ii} terms:

$$k_{ii} \geqslant \eta_i + \sum_{j=1}^{3} |\bar{k}_{ij}\,\tilde{x}_{rj}| + |\tilde{x}_{ri+3}| \quad i = 1,\ 2,\ \text{and } 3. \tag{23}$$

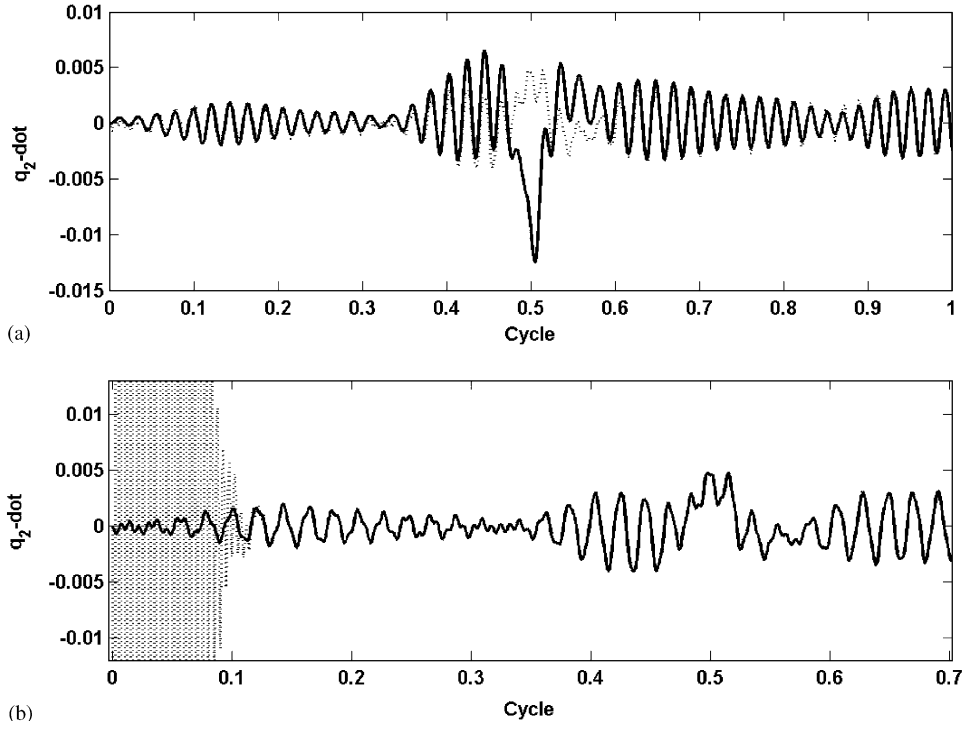

Fig. 7. $\dot{q}_2$ of the crankshaft from case 1. (a) Exact (——) and measured (……), (b) measured (——) and estimated (……).

When the system is located on the sliding surface, its dynamics are governed by

$$\dot{\underset{\sim}{s}} = (\nabla \underset{\sim}{s})\,\dot{\underset{\sim}{\tilde{x}}}_r = \begin{bmatrix} I_{3\times 3} & 0_{3\times 3} \end{bmatrix} \dot{\underset{\sim}{\tilde{x}}}_r = C\left[\underset{\sim}{\Delta f}_r - \bar{k}\begin{pmatrix} \tilde{x}_{r1} \\ \tilde{x}_{r2} \\ \tilde{x}_{r3} \end{pmatrix} - k\begin{pmatrix} \mathrm{sgn}(\tilde{x}_{r1}) \\ \mathrm{sgn}(\tilde{x}_{r2}) \\ \mathrm{sgn}(\tilde{x}_{r3}) \end{pmatrix}\right] = \underset{\sim}{0} \tag{24}$$

Ideally, $\tilde{x}_{ri}$ must be zero when the system is located on the ith sliding surface. However, due to disturbances and model uncertainties, the system may leave the sliding surface; thus, causing $\tilde{x}_{ri}$ to become different than zero. Ignoring the terms associated with $\bar{k}$, the $\mathrm{sgn}(\tilde{x}_{ri})$ terms can be written as

$$[\mathrm{sgn}(\tilde{x}_{r1})\ \mathrm{sgn}(\tilde{x}_{r2})\ \mathrm{sgn}(\tilde{x}_{r3})]^{\mathrm{T}} = (Ck)^{-1} C\,\underset{\sim}{\Delta f}_r\,. \tag{25}$$

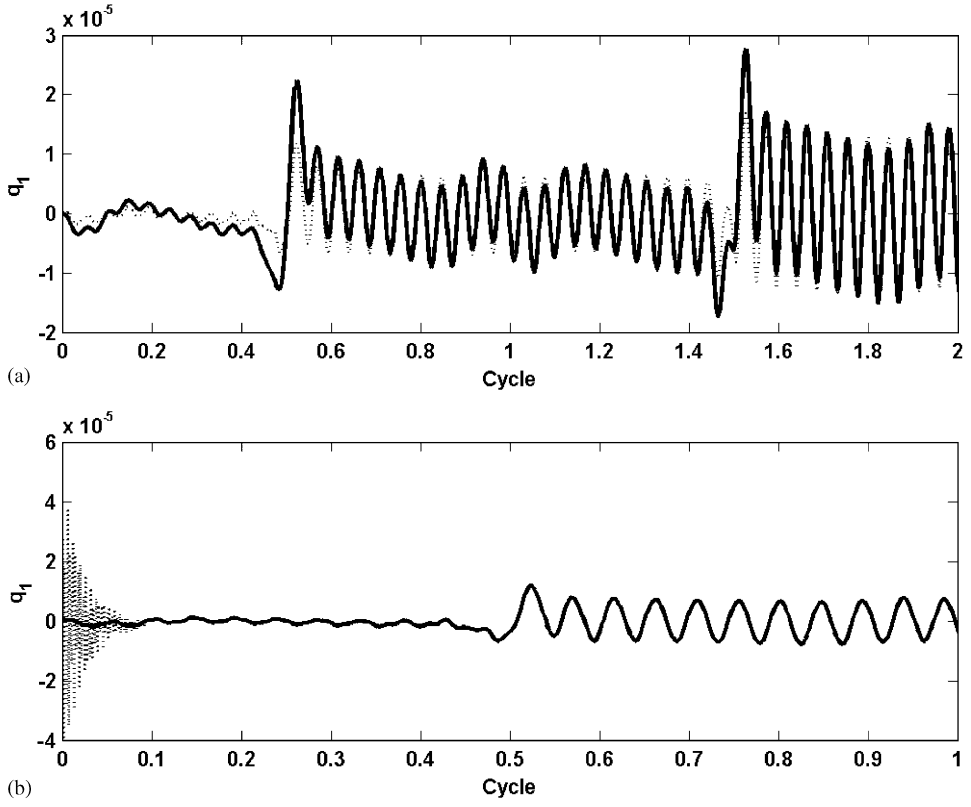

Fig. 8. First elastic mode of the crankshaft from case 2. (a) Exact (——) and measured (… …), (b) measured (——) and estimated (… …).

Combining Eqs. (19) and (25), the vector error equation, describing the system behavior during the sliding mode, becomes

$$\dot{\tilde{\underset{\sim}{x}}}_r = (I - k(Ck)^{-1}C)\,\Delta\underset{\sim}{f}_r$$

$$= \begin{pmatrix} 0 & 0 & 0 & 0 & 0 & 0 \\ 0 & 0 & 0 & 0 & 0 & 0 \\ 0 & 0 & 0 & 0 & 0 & 0 \\ 0 & 0 & 0 & -\frac{k_{41}}{k_{11}} & -\frac{k_{42}}{k_{22}} & -\frac{k_{43}}{k_{33}} \\ 0 & 0 & 0 & -\frac{k_{51}}{k_{11}} & -\frac{k_{52}}{k_{22}} & -\frac{k_{53}}{k_{33}} \\ 0 & 0 & 0 & -\frac{k_{61}}{k_{11}} & -\frac{k_{62}}{k_{22}} & -\frac{k_{63}}{k_{33}} \end{pmatrix} \tilde{\underset{\sim}{x}}_r + \begin{pmatrix} 1 & 0 & 0 \\ 0 & 1 & 0 \\ 0 & 0 & 1 \end{pmatrix} \begin{Bmatrix} \Delta f_{r4} \\ \Delta f_{r5} \\ \Delta f_{r6} \end{Bmatrix}. \tag{26}$$

In this study, all off-diagonal terms in the above equation have been set to zero. Therefore, for an asymptotically stable response of the homogeneous parts of the $\tilde{x}_{r4}$, $\tilde{x}_{r5}$ and $\tilde{x}_{r6}$ differential

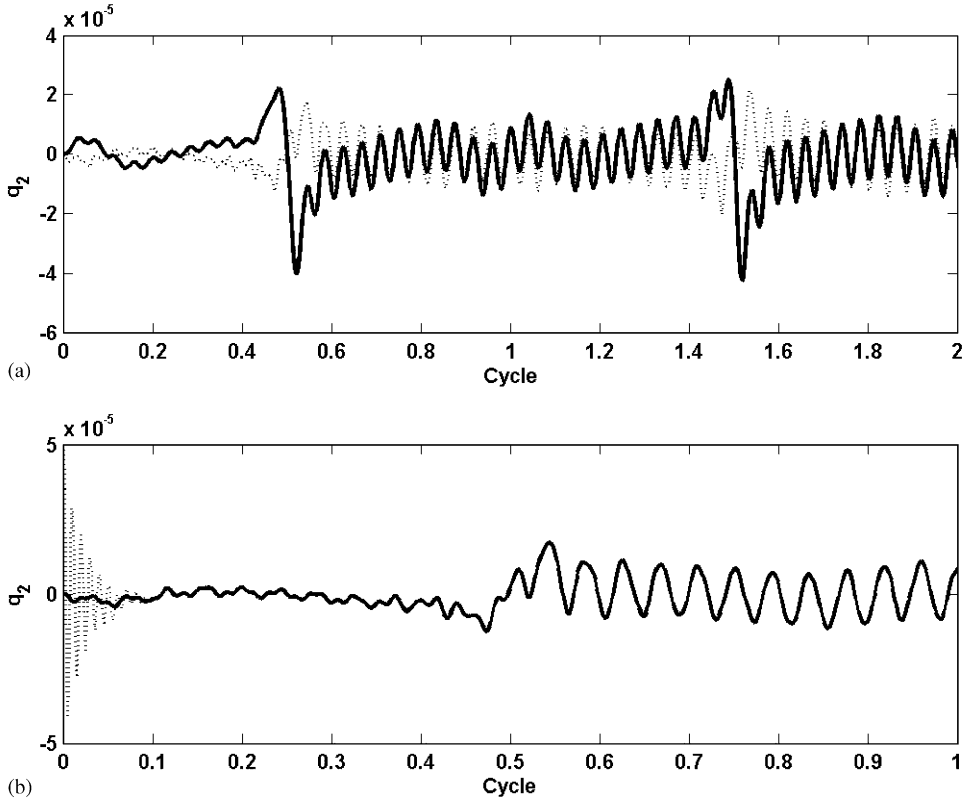

Fig. 9. Second elastic mode of the crankshaft from case 2. (a) Exact (——) and measured (……), (b) measured (——) and estimated (……).

equations, k_{41}/k_{11}, k_{52}/k_{22} and k_{63}/k_{33} must be positive. However, according to Eq. (23), the k_{ii} terms take on positive numerical values. This causes k_{41}, k_{52} and k_{63} to be positive.

Due to the unavailability of $\tilde{x}_{r4}$, $\tilde{x}_{r5}$ and $\tilde{x}_{r6}$, a feedforward compensation is implemented herein based on upper bounds of modeling uncertainties and error variables. For instance, in the computation of the k_{ii} gains as defined in Eq. (23), both η_i and $\bar{k}_{ij}$ are considered to be known quantities because they are assigned by the designer. Moreover, $\tilde{x}_{r1}$, $\tilde{x}_{r2}$ and $\tilde{x}_{r3}$ are available through direct measurements. The remaining unknown terms $\tilde{x}_{r4}$, $\tilde{x}_{r5}$ and $\tilde{x}_{r6}$ are selected to be the desired upper bounds of the error in the estimation of x_{r4}, x_{r5} and x_{r6}. This yields the following expression for the k_{ii} gain term:

$$k_{ii\ \text{upper\_bound}} \geqslant \eta_i + \sum_{j=1}^{3} |\bar{k}_{ij}\ \tilde{x}_{rj}| + |\tilde{x}_{ri+3}|_{\text{desired\ \ upper\_bound}} \quad i = 1,\ 2,\ \text{and}\ 3. \tag{27}$$

Similarly, k_{41}, k_{52} and k_{63} are determined as follows:

$$k_{(i+3)(i)\text{upper\_bound}} = k_{ii\text{upper\_bound}} \frac{\text{Educated guess on } (\Delta f_{r(i+3)})_{\max}}{(\tilde{x}_{r(i+3)})_{\text{desired\ \ upper\_bound}}} \quad i = 1,\ 2,\ \text{and}\ 3. \tag{28}$$

Note that $\bar{k}$, has been treated thus far as a known quantity. It represents the Luenberger observer gain matrix, which is determined based on the $\bar{A}$ and $\bar{B}$ matrices obtained by linearizing

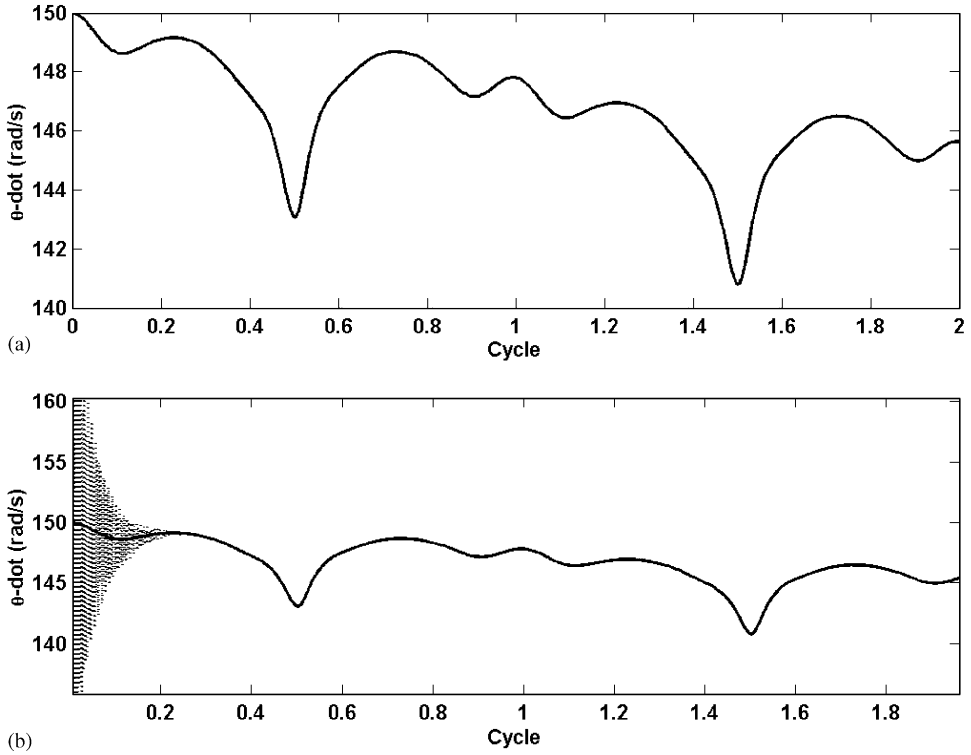

Fig. 10. Angular velocity of the crankshaft from case 2. (a) Exact (——) and measured (… …), (b) measured (——) and estimated (… …).

Eq. (13) around $\hat{x}_{re} = \underset{\sim}{0}$. It should be stressed that the $\bar{k}[\,\tilde{x}_{r1} \quad \tilde{x}_{r2} \quad \tilde{x}_{r3}\,]^{\mathrm{T}}$ term provides additional corrective action that aids the system in reaching the sliding surface.

4. Assessment of the observer in estimating the rigid and flexible motions of the crankshaft

Throughout this work, a constant load torque and a force, based on experimental data of a cylinder gas pressure, have been used (see Fig. 2). Both T_{load} and P_{gas} are used in the detailed model, described in Section 2, to determine the exact values for the friction torque, T_f, and the combined rigid and flexible motions of the crank-slider mechanism. It should be emphasized that the exact values are used herein as a base for comparison in the assessment of the observer. Moreover, they are needed for determining the measured signals, y_i's, which are defined in Eqs. (14) and (16).

Two cases, reflecting transient operating conditions that involve a decrease in the engine speed, have been considered in the assessment of the observer performance. The initial conditions, selected in both cases, for the detailed model and the nominal model of the crank-slider mechanism are:

$$\text{Case 1 (700 rpm)}: \quad \underset{\sim}{x}(0) = (0,0,0,0,0,0,0,73.3,98.04,24.74,0,0,0,0)^{\mathrm{T}}$$
$$\underset{\sim}{x_r}(0) = (0,0.00005,0.00005,100,0,0)^{\mathrm{T}} \tag{29a}$$

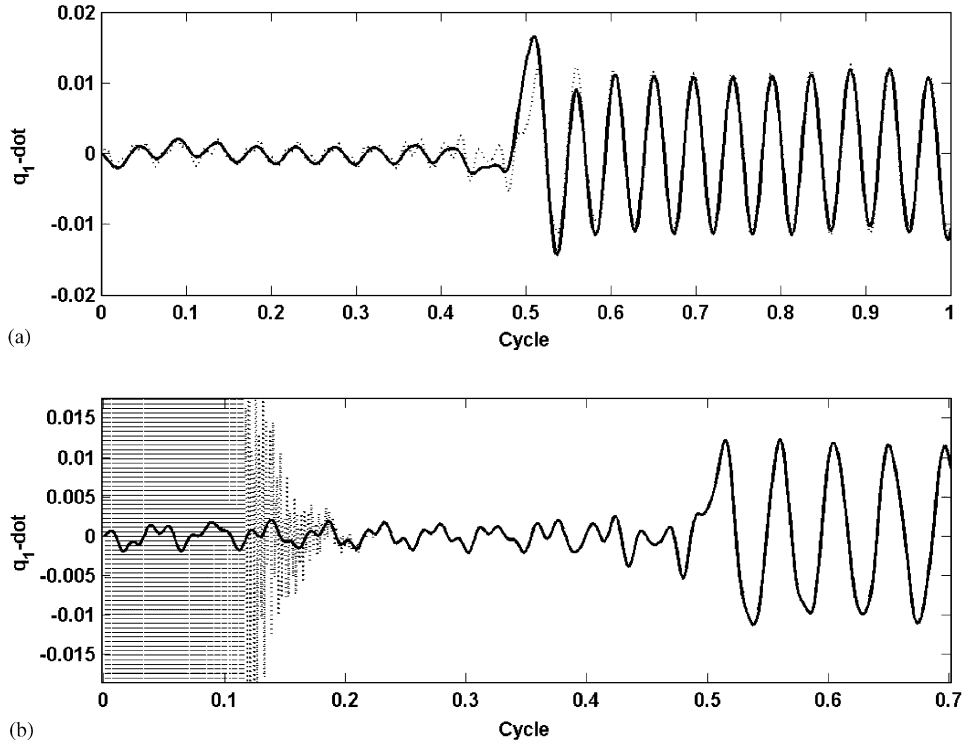

Fig. 11. $\dot{q}_1$ of the crankshaft from case 2. (a) Exact (——) and measured (……), (b) measured (——) and estimated (……).

$$\text{Case 2 (1432 rpm)}: \quad \underset{\sim}{x}(0) = (0,0,0,0,0,0,0,150,200.63,50.63,0,0,0,0)^{\mathrm{T}}$$
$$\underset{\sim}{x}_r(0) = (0,0.00005,0.00005,125,0,0)^{\mathrm{T}} \tag{29b}$$

Case 1 corresponds to an initial engine speed of 700 rpm. Its results are shown in Figs. 3–7. Note that part (a) of each figure provides a comparison between the exact value of the state variable, as generated by the detailed model of the crank-slider mechanism, and its "measured" counterpart as defined by Eqs. (15) and (16). The deviations of q_{1_m}, q_{2_m}, $\dot{\theta}_m$, $\dot{q}_{1_m}$ and $\dot{q}_{2_m}$ from their exact values illustrate the errors introduced in the "measured" state variables by ignoring the higher order dynamics of the crankshaft. Moreover, parts (b) of Figs. 3–7 reveal a rapid convergence of q_{1_e}, q_{2_e}, $\dot{\theta}_e$, $\dot{q}_{1_e}$ and $\dot{q}_{2_e}$ to their respective "measured" state variables; thus, demonstrating a good and robust performance of the observer in the presence of both structured and unstructured uncertainties.

Case 2 corresponds to an initial engine speed of 1432 rpm, which is significantly higher than the one considered in case 1. The results are shown in Figs. 8–12. They exhibit a similar trend in the performance of the observer as in the previous case. Note that the rapid convergence rate of the observer was preserved in case 2 in spite of larger uncertainties, higher inertial forces and larger structural deformations than those encountered in case 1.

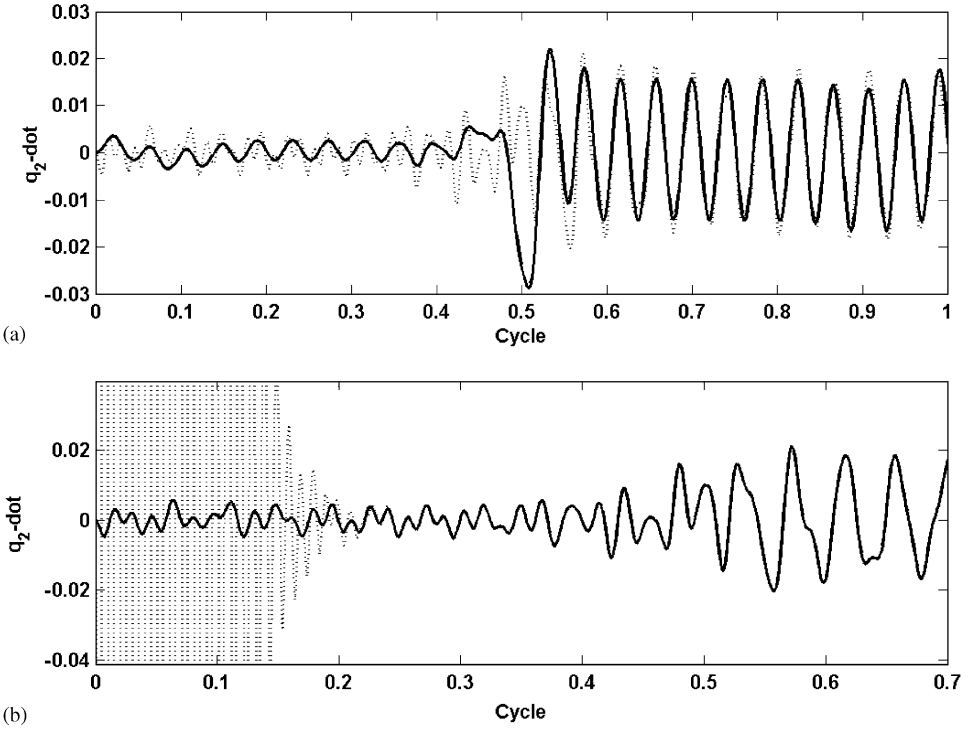

Fig. 12. $\dot{q}_2$ of the crankshaft from case 2. (a) Exact (——) and measured (……), (b) measured (——) and estimated (……).

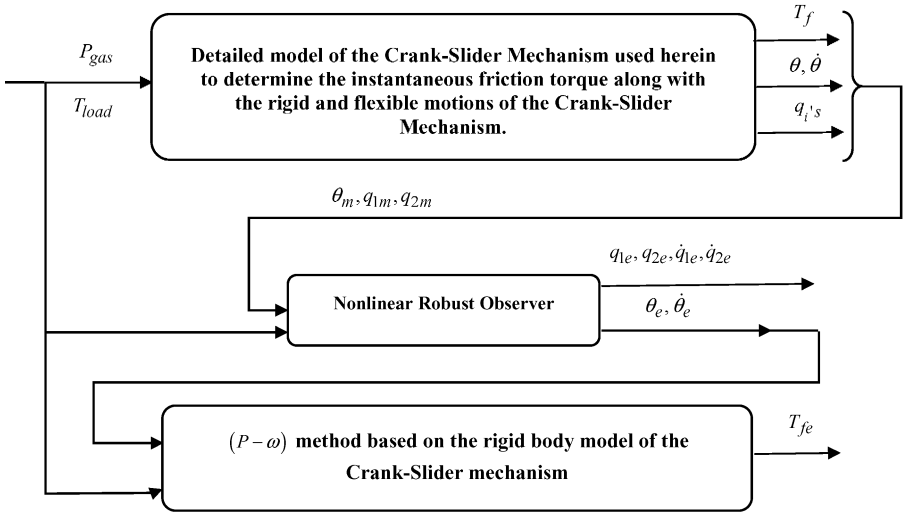

Fig. 13. Proposed scheme for implementing a nonlinear observer to enhance the accuracy of the $(P-\omega)$ method.

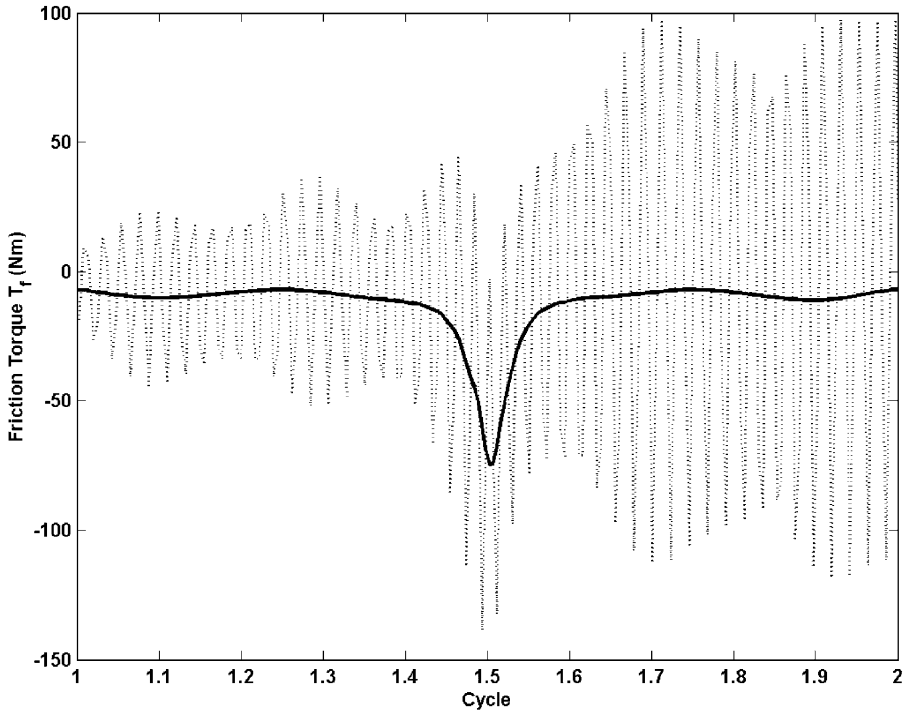

Fig. 14. Instantaneous friction torques generated by the detailed model, T_f (——), and by the $(P-\omega)$ method based on measured state variables, T_{fc} (……), from case 1.

5. Enhancement of the accuracy of the (P–ω) method by the implementation of a nonlinear observer

The ($P-\omega$) method determines the instantaneous engine friction torque based on the measured cylinder gas pressure, the engine load torque, the angular displacement of the crankshaft and its time derivatives. Its formulation, which is inserted in the lower block of Fig. 13, is obtained from the rigid body model of the crank-slider mechanism. By implementing the substitution method to eliminate the superfluous β and γ coordinates, the rigid body model of the crank-slider mechanism can be reduced to the following differential equation in θ:

$$J(\theta)\ddot{\theta} + \bar{F}(\theta, \dot{\theta}) = G(P_{\text{gas}}, T_{\text{load}}) + T_f, \tag{30}$$

where all the friction terms are represented by T_f. The ($P-\omega$) method uses the above equation as an algebraic one to compute the instantaneous engine friction torque. The substitution of the measured $P_{\text{gas}}, T_{\text{load}}, \theta$ and its time derivatives into Eq. (30) renders all the terms to become known quantities except for T_f. It should be stressed that the ($P-\omega$) method does not have any provision in its formulation to account for the structural deformations. Therefore, the numerical values of θ and its derivatives, needed for the computation of the friction torque, should solely represent the rigid body motion of the crankshaft. Otherwise, this method would lead to

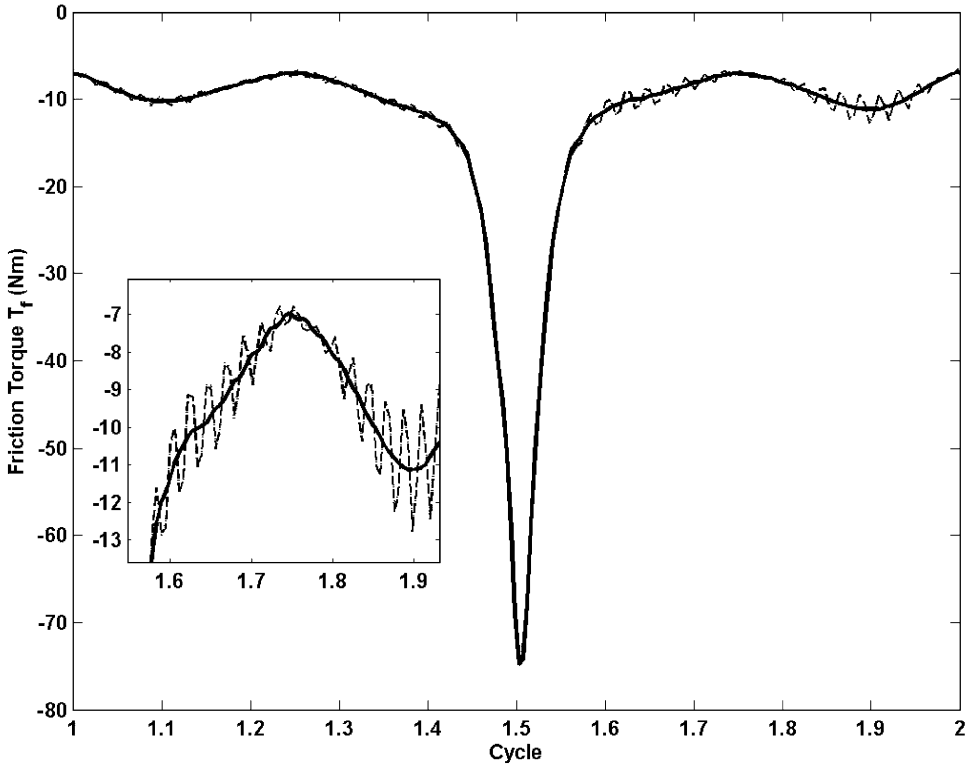

Fig. 15. Instantaneous friction torques generated by the detailed model, T_f (——), by the ($P-\omega$) method based on exact state variables, T_{fa} (- - - -), and by the ($P-\omega$) method based on estimated state variables, T_{fe} (……), from case 1.

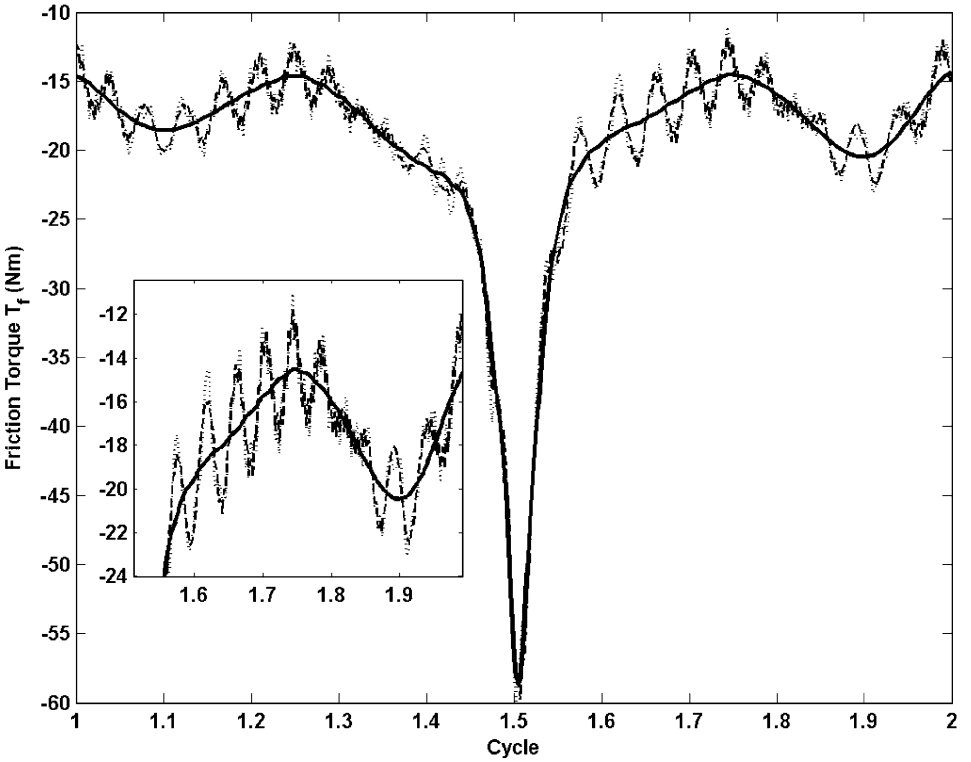

Fig. 16. Instantaneous friction torques generated by the detailed model, T_f (——), by the $(P-\omega)$ method based on exact state variables, T_{fa} (- - - -), and by the $(P-\omega)$ method based on estimated state variables, T_{fe} (……), from case 2.

erroneous friction results as shown in Fig. 14 [6]. Note that the curve T_f represents the exact engine friction torque generated by the detailed model of the crank-slider mechanism. It is used herein as a basis for comparison. Whereas, T_{fc} is the engine friction torque determined by using the measured angular displacement of the crankshaft, y_1, and its time derivatives in the $(P-\omega)$ method. Fig. 14 shows that T_{fc} undergoes large oscillations around T_f, which causes it to assume positive numerical values.

To address this problem, the nonlinear observer, inserted in the center block of Fig. 13, is used in this work to provide accurate estimates of θ and its derivatives. Figs. 5 and 10 illustrate a rapid convergence of $\dot{\theta}_e$ to $\dot{\theta}_m$ in both cases 1 and 2. Similar trend of rapid convergence has been observed between θ_e and θ_m. However, these results are not shown here due to the limited space. Figs. 15 and 16 illustrate the instantaneous friction torques corresponding to cases 1 and 2, respectively. Note that both T_{fa} and T_{fe} curves are determined by the $(P-\omega)$ method. The former was computed based on θ and its time derivatives, as generated by the detailed model of the crank-slider mechanism, while the latter was determined based on the estimated state variables. Figs. 15 and 16 reveal slight differences between T_{fa} and T_{fe}. However, they demonstrate that the difference between T_f and the other friction curves becomes more pronounced in case 2 than in case 1. This is because the detailed model, based on which T_f is generated, retains all the coupling

terms between the rigid and flexible motions. However, both T_{fa} and T_{fe} are determined by the $(P-\omega)$ method, which only accounts for the rigid body motion of the crank-slider mechanism. The effects of the flexible motion on the rigid body motion, which are ignored in the $(P-\omega)$ method, become increasingly important as the engine speed is increased. This is clearly manifested by the oscillations of T_{fa} and T_{fe} around T_f, whose magnitudes become significantly larger as the engine speed increases from 700 rpm in case 1 to 1432 rpm in case 2.

6. Summary and conclusions

A nonlinear sliding mode observer has been developed in this study to accurately estimate the rigid and flexible motions of the piston-assembly/connecting-rod/crankshaft mechanism of a single cylinder engine. The observer is designed to yield a robust performance in the presence of both structured and unstructured uncertainties.

The digital simulation results illustrate the robust performance of the observer through the rapid convergence of the estimated state variables to the actual ones. This performance was demonstrated under transient operating conditions representing a decrease in the engine speed.

Moreover, the simulation results have proven that the use of the estimated rather than the measured angular displacement of the crankshaft and its time derivatives can significantly improve the accuracy of the $(P-\omega)$ method in determining the instantaneous engine friction torque.

Future steps will involve experimental work aimed at validating the theoretical results presented in the current study.

Acknowledgments

The authors would like to acknowledge the financial support of the Automotive Research Center (consortium of eight universities directed by the University of Michigan) sponsored by the National Automotive Center, located within the US Army Tank-Automotive Research, Development, and Engineering Center (TARDEC), Warren, Michigan and by the US Army Research Office (ARO), North Carolina.

References

[1] N.A. Henein, Instantaneous engine frictional torque, its components and piston assembly friction, Technical Report, Mechanical Engineering Department, Wayne State University, 1992.

[2] S. Furuhama, K. Machidam, M. Takiguchi, Piston friction force of a small high speed gasoline engine, *Transaction of the ASME 1988* 110 (1988) 112–118.

[3] K. Shin, Y. Tateishi, S. Furuhama, Measurement and characteristics of instantaneous piston ring frictional force, *1985 ASME International Mechanical Engineering Congress and Exposition* 3 (1985) 87–94.

[4] H.M. Uras, D.J. Patterson, Measurement of piston and ring assembly friction instantaneous IMEP method, *SAE Paper* 830416 (1983).

[5] N.A. Henein, A. Fragoulis, A. Nichols, Time-dependent frictional torque in reciprocating internal combustion engines, *Journal of the Society of Tribologists and Lubrication engineers* 44 (1988) 313–318.
[6] N.G. Chalhoub, H.K. Nehme, N.A. Henein, W. Bryzik, Effects of structural deformations of the crank-slider mechanism on the estimation of the instantaneous engine friction torque, *Journal of Sound and Vibration* 224 (3) (1999) 489–503.
[7] H.K. Nehme, N.G. Chalhoub, N.A. Henein, Effects of filtering the angular motion of the crankshaft on the estimation of the instantaneous engine friction torque, *Journal of Sound and Vibration* 236 (5) (2000) 881–894.
[8] D. Taraza, N.A. Henein, W. Bryzik, Experimental determination of the instantaneous frictional torque in multi-cylinder engines, *SAE Paper* 962006 (1996).
[9] H. Yanada, M. Shimahara, Sliding mode control of an electrohydraulic servo motor using a gain scheduling type observer and controller, *1997 ASME International Mechanical Engineering Congress and Exposition, Proceedings of the Institution of Mechanical Engineers* 211 (I) (1997) 407–416.
[10] M.H. Kim, D.J. Inman, Reduction of observation spillover in vibration suppression using a sliding mode observer, *Journal of Vibration and Control* 7 (2001) 1087–1105.
[11] B.L. Walcott, S.H. Zak, Observation of dynamical systems in the presence of bounded nonlinearities/uncertainties, *Proceedings of the 25th Conference on Decision and Control*, Athens, Greece, 1986.
[12] J.J.E. Slotine, J.K. Hedrick, E.A. Misawa, On sliding observers for nonlinear systems, *Journal of Dynamic Systems, Measurement, and Control* 109 (1987) 245–252.
[13] E.A. Misawa, J.K. Hedrick, Nonlinear observers—A state-of-the-art survey, *Journal of Dynamic Systems, Measurement, and Control* 111 (1989) 344–352.
[14] N.G. Chalhoub, G.A. Kfoury, Development of a robust nonlinear observer for a single-link flexible manipulator, *Nonlinear Dynamics* 39 (2005) 217–233.
[15] S.F. Rezeka, N.A. Henein, A new approach to evaluate instantaneous friction and its components in internal combustion engines, *SAE Paper* 840179 (1984).
[16] L. Meirovitch, *Elements of Vibration Analysis*, McGraw-Hill, New York, 1986.
[17] H.K. Nehme, N.G. Chalhoub, N.A. Henein, Development of a dynamic model for predicting the rigid and flexible motions of the crank slider mechanism, *ASME Journal of Engineering for Gas Turbines and Power* 120 (3) (1998) 678–686.
[18] H.K. Nehme, Role of structural deformations of the crank-slider mechanism in the computation of the instantaneous frictional losses of a single cylinder engine, Ph.D. Dissertation, Mechanical Engineering Department, Wayne State University, 2000.
[19] D. Young, R.P. Felgar, *Tables of characteristic functions representing normal modes of vibration of a beam*, Vol. 4913, The University of Texas, Publication, 1949.
[20] C. Glocker, F. Pfeiffer, Dynamical systems with unilateral contacts, *Nonlinear Dynamics* 3 (1992) 245–259.
[21] C.W. Gear, *Numerical Initial Value Problems in Ordinary Differential Equations*, Prentice-Hall, Englewood Cliffs, NJ, 1971.